# Structural and dynamic properties of aluminosilicate melts: a molecular dynamics study

Mohammed Bouhadja, Noël Jakse

# Structural and Dynamic Properties of Aluminosilicate Melts: A Molecular Dynamics Study

Mohammed Bouhadja[1] and Noël Jakse[2]

[1] *Institut des Molécules et Matériaux du Mans (Faculté des sciences) Université Nantes-Angers-Le Mans, 72085 Le Mans Cedex 09, France*

[2] *Univ. Grenoble Alpes, CNRS, Grenoble INP, SIMaP, F-38000 Grenoble, France*

(Dated: July 1, 2020)

## Abstract

In the present work, the structural and dynamic properties of aluminosilicates $(Al_2O_3)_x$-$(SiO_2)_{1-x}$ (AS) as a function of the $Al_2O_3$ concentration $x$ are studied by means of molecular dynamics simulations. Firstly, the parametrization of the Born-Mayer-Huggins type potential developed recently for the more general CaO-$Al_2O_3$-$SiO_2$ ternary system is assessed. Comparison of local structural properties, such as the X-ray structure factor, partial pair-correlation functions, distributions of coordination numbers and bond angles, as well as the dynamics through the viscosity and self-diffusion coefficients to experimental data and other molecular dynamics simulations found in the literature, shows that this potential is transferable to AS melts for all compositions and is more reliable than other empirical potentials used so far. The evolution of viscosity with temperature in stable liquid and undercooled regions is studied in the whole composition range and results show a progressive increase of the fragility with increasing $Al_2O_3$ content correlated to that of local structural entities like the triply bonded oxygen (TBO), $AlO_5$ and $AlO_6$.

## I. INTRODUCTION

Understanding physical properties of silicate-based glasses is of utmost importance not only regarding fundamental aspects in Materials and Earth Sciences[1], but also to address future technological, energetic, and environmental challenges in glass-making, nuclear waste storage and cement industries[2]. They are most often produced from the melt so that control of their casting requires a deep understanding of properties and their evolution from the liquid state down to the glass transition temperature $T_G$, through the undercooled state. In particular, an accurate knowledge of the microscopic structural properties is needed, as they are known to impacts dynamics and mass transport properties such as the diffusion and viscosity[3–12].

The aluminosilicate system $(Al_2O_3)_x$-$(SiO_2)_{1-x}$ (AS), where $x$ represents the alumina content, is of particular interest since it represents the binary mixture from which many silicate glasses are formed[13–15], and for instance the archetypal CaO-$Al_2O_3$-$SiO_2$ (CAS) glass[16]. It is composed of two interpenetrating tetrahedral network namely, $SiO_2$ and $Al_2O_3$ networks connected *via* common corner-sharing O atoms, so-called bridging oxygen (BO). While the silica network is known to be a strong tetrahedral network, the alumina one appears to be looser with a more complex oxygen atom arrangement around aluminium. In this respect, experimental investigation of the microscopic structural properties, using Nuclear Magnetic Resonance[17–19,21–23] as well as combined Infrared, X-Ray and Raman Spectroscopy[24–26] were oriented towards the understanding of the local environment around Al atoms. Charge neutrality expected in the AS system, indeed impose a local ordering of $O^{2-}$ anions around $Al^{3+}$ cations different to the $Si^{4+}$ ones. These studies have then inferred the possibility that the coordination of O atoms around Al can be higher than 4, namely, 5 and even 6. Such a complex structure induces the production of a significant amount of triply bonded oxygen (TBO) atoms with cations, also called triclusters, which might become larger as the $Al_2O_3$ content increases[27]. We may anticipate that the presence of these structural entities, namely $AlO_n$ and TBO, have significant effects on dynamics of AS melts, as was already shown in the case of CAS for the diffusion and the viscosity[28,29]. Moreover, non-bonded free oxygen (NBO) atoms have been reported in AS glasses[30–32].

These defects at the atomic scale are most of the time hardly accessible from experiments[9]. Then, molecular dynamics (MD)[33,34] represents a reliable alternative to get a better under-

standing of the atomic scale behavior and their relation with macroscopic properties, provided that simulations are performed with realistic interatomic interactions. A very accurate description of these interactions can be obtained obviously by *ab initio* MD, but simulations that can be carried out are limited in size and length scales due to the large computational cost, impeding systematic studies. After the first simulations reported for AS melts with the Born-Mayer type potentials[18,19], most MD simulations[35–39,41,46] were performed using Kramer *et al.*[42] model derived from the famous BKS potentials[43]. Interestingly, another strategy has been followed very recently[51], consisting in extracting potentials for AS binary system which was primarily designed in the context of the ternary CAS system[28,45]. The resulting potential has however to be assessed for each case study, due to possible lack of transferability.

Moreover, only very few studies have been devoted to the evolution of structural and thermodynamic properties as a function of composition and temperatures down to the undercooled and glassy states[35,36,38,39,41]. These simulation studies have pointed out remarkable structural features such as micro-segregation associated to Al-rich channels percolating through the Si-O, as well as triclusters as important features of atomic transport and chemical disorder of the covalent-bonded network. Other studies have indicated the presence of a fragile-to-strong transition from the non-Arrhenius-to-Arrhenius crossover in the undercooled region and an increase of dynamic heterogeneities (DH). However, a complete study of these features as function of composition and temperature for AS melts, and their link with fragility, is still missing, as only few compositions have been considered so far. Moreover, as these features can hardly be observed experimentally, their study by atomistic simulations with accurate potentials is therefore of great importance.

In the present work, we have studied the evolution of structural and dynamic properties of $(Al_2O_3)_x$-$(SiO_2)_{1-x}$ as a function of $Al_2O_3$ concentration $x$ varying 0 to 1 by means of classical molecular dynamics. Interactions are modelled from the Born-Mayer-Huggins (BMH) type potential whose parameters were recently optimized by Bouhadja *et al.* for the CAS melts[16,28,29] and shown to be efficient in describing their structural feature and atomic transport properties. In a first part, we test ability of this potential to describe the structure as function of alumina content by comparing then with X-ray diffraction data[50]. Given the quality and transferability of the potential in the whole concentration range, in a second part, we examine structural entities such as $AlO_n$, TBO and triclusters, and their

impact on the dynamics properties such as diffusion, viscosity and fragility as a function of concentration. Our findings show a strong correlation between them.

The layout of the paper is the following. In the next Section, the technical background of our work is described in some details. In Section III, the results of our simulations are presented and discussed. Finally, conclusions are given in Section IV .

## II. SIMULATION BACKGROUND

Atomic interactions in the $(Al_2O_3)_x$-$(SiO_2)_{1-x}$ glass-formers have been chosen in the form of the Born-Mayer-Huggins potential[44], called hereafter BMH, for which interactions between Al, Si and O atoms are given by

$$V(r_{ij}) = \frac{q_i q_j}{r_{ij}} + A_{ij} exp\left(\frac{\sigma_{ij} - r_{ij}}{\rho_{ij}}\right) - \left(\frac{C_{ij}}{r_{ij}}\right)^6 - \left(\frac{D_{ij}}{r_{ij}}\right)^8, \quad (1)$$

with $i$ and $j$ = Si, Al, O and $r$ being the interatomic distance between two ions of species $i$ and $j$. The first term represents the long-range Coulomb potential involving charges $q_i$ and $q_j$. The second term is the Born repulsive term which results from electronic overlap of neighboring atoms, while the two last contributions are the two first terms of the dipolar expansion, though here we take only the van der Waals term into account. Parameters in Eq. (1) are given in Table I and readily taken from the potentials used successfully to describe the CAS ternary system[52,53] proposed by Bouhadja *et al.*[16,28,29].

For the purpose of studying the structural and dynamic properties of AS melts in the whole range of $Al_2O_3$ concentration, we have performed classical molecular dynamics simulations with the BMH potential using the LAMMPS code[54]. The number of atoms in the simulation box for each system AS$y$, with $y = 100x$ the percentage of $Al_2O_3$, are given in Table II. The equations of motion were solved numerically within Verlet algorithm in the velocity form[33,34] using a time step of 1 fs. From a thermodynamic point of view, all the simulations were performed in the isobaric-isothermal ensemble (NPT) with zero pressure. In a first stage, we equilibrated the system for 100 ps at a temperature $T = 6500$ K from an initial configuration with random atomic positions. Then, we cooled down system with cooling rate of $10^{11}$ K/s up to $T = 300$ K, and configurations were stored regularly during this process. At intervals of 500 K, we took the corresponding configuration and brought the system to equilibrium for a period of 10 ns at constant temperature and pressure. The

| | $q$ | $A$ (eV) | $\rho$ (Å) | $\sigma$ (Å) | $C$ (eVÅ$^6$) |
|---|---|---|---|---|---|
| Al | 1.8 | | | | |
| O | −1.2 | | | | |
| Si | 2.4 | | | | |
| Al-Al | | 0.0029 | 0.0680 | 1.5704 | 14.0498 |
| Al-O | | 0.0075 | 0.1640 | 2.6067 | 34.5747 |
| O-O | | 0.0120 | 0.2630 | 3.6430 | 85.0840 |
| Si-O | | 0.0070 | 0.1560 | 2.5419 | 46.2930 |
| Al-Si | | 0.0025 | 0.0570 | 1.5056 | 18.8116 |
| Si-Si | | 0.0012 | 0.0460 | 1.4408 | 25.1873 |

TABLE I: Parameters for the AS potentials taken from[16,28,29] (see Eq. 1).

structure and dynamic properties were then produced for time spans guaranteeing sufficient statistics (up to 200 ns at the lowest temperatures in the undercooled states, as in our preceding work on CAS[29]).

The study of the short-range order was first based on the partial pair-correlation functions $g_{ij}(r)$, giving the probability of finding a particle $j$ at distances $r$ relative to a particle $i$ located at the origin, namely:

$$g_{ij}(r) = \frac{N}{V}\frac{n_{ij}(r)}{4\pi r_{ij}^2 \Delta r}. \tag{2}$$

$n_{ij}(r)$ represents the mean number of particles $j$ in a spherical shell of radius $r$ and thickness $\Delta r$ centered on particle $i$. The first minimum of each $g_{ij}(r)$ defines a cutoff radius that will serve to determine the coordination numbers and all the structural quantities such as the NBO, TBO and $AlO_n$. In this context, we have used the ISAACS software[55] to determine these quantities as well as the total X-ray pair-correlation functions and resulting structure factors.

Concerning the dynamics, we determined the self-diffusion coefficient $D_i$ of each species from the linear behavior at long times of the mean-square displacement

| | Al | O | Si |
|---|---|---|---|
| $SiO_2$ | – | 670 | 335 |
| AS10 | 62 | 651 | 279 |
| AS20 | 116 | 638 | 232 |
| AS30 | 168 | 644 | 196 |
| AS40 | 208 | 618 | 156 |
| AS50 | 250 | 625 | 125 |
| AS60 | 288 | 624 | 96 |
| AS70 | 322 | 621 | 69 |
| AS80 | 352 | 616 | 44 |
| AS90 | 360 | 520 | 80 |
| $Al_2O_3$ | 414 | 621 | – |

TABLE II: Number of atoms of each atom type for all compositions AS$y$, with $y = 100x$ the percentage of $Al_2O_3$.

$$R_i^2(t) = \frac{1}{N}\sum_{l=1}^{N_i}\left\langle [\mathbf{r}_l(t+t_0) - \mathbf{r}_l(t_0)]^2 \right\rangle_{t_0}, \tag{3}$$

where $\mathbf{r}_l(t)$ denotes the position of atom $l$ at time $t$ and $N_i$ is the number of particles of species $i$.

We have also calculated the viscosity by means of the Reverse Non-Equilibrium Molecular Dynamics (RNEMD) method[56,57]. At each desired temperature, after equilibration, we performed an additional simulation in the canonical ensemble (NVT) in which the simulation box is divided in 20 slabs with the same thickness. The momentum of atoms is reversed every 20 time steps over a period $10^7$ time steps. The momentum and the simulation time in the interval of exchange were optimized beforehand by realizing trial simulation run to achieve a steady state and a linear velocity profile. We refer the reader to our preceding work for more details[29]. It's worth mentioning that for all compositions at very low temperature, the shear viscosity shows large values with velocity profile almost flat. We avoided calculating the viscosity as soon as an accurate estimate could not be obtained anymore in a reasonable calculation time.

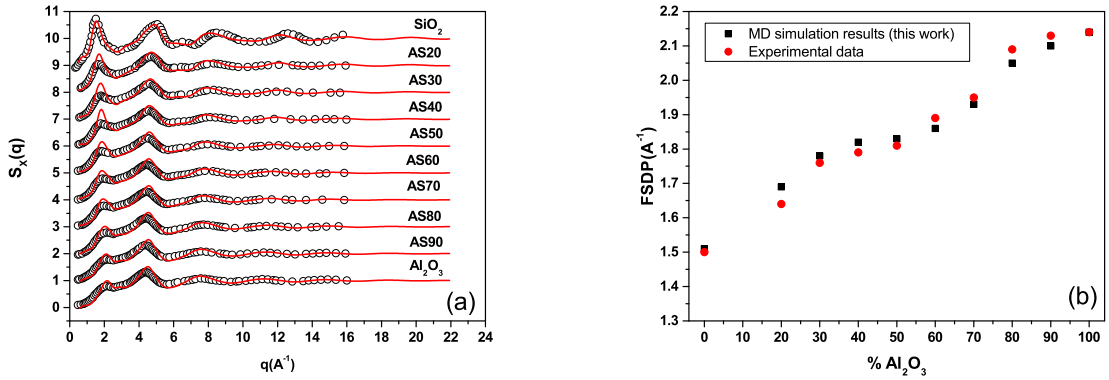


FIG. 1: (a) Total structure factor from X-ray diffraction at $T = 2300$ K for all the compositions AS$y$, with $y = 100x$ the percentage of $Al_2O_3$, at $T = 2400$ K for pure $Al_2O_3$ at $T = 2300$ K and for all other As$y$ systems[59]. The open circles are the experimental data of Wilding *et al.*[50] and Skinner *et al.*[59], while the full red lines are the simulation data of the present work. (b) First sharp diffraction peak (FSDP) position as a function of $y$ from experiment (red full squares) and MD simulations of the present work (black full squares).

## III. RESULTS AND DISCUSSION

### A. Structural properties

In a first step, the ability of the BMH potential to reproduce the experimental X-ray structure factors is assessed. Figure 1(a) shows a comparison of our MD simulations with the experimental data of Wilding *et al.*[50] in the liquid state. For wave-vectors $q > 3$ Å$^{-1}$, namely for the short-range order, MD simulations are in excellent agreement with the experimental data for all composition including the pure $SiO_2$ and $Al_2O_3$. The good agreement extends to the medium-range order, in particular in the vicinity of the First Sharp Diffraction Peak (FSDP) for $q < 2.5$ Å$^{-1}$). Its position reproduces closely the experimental evolution with $Al_2O_3$ composition in the whole range of $x$ as can be seen in Figure 1(b). Moreover, the amplitude of the simulated FSDP, albeit being sightly overestimated especially in the $Al_2O_3$ poor region, reproduce the experimental trend showing a decrease with composition and therefore a progressive loss of intermediate range ordering.

Fig. 2(a) shows the total X-ray radial distribution functions for compositions AS30, AS50, and AS70 from our simulations with the BMH potential together with experimental

| | First peak position (Å) | | | Second peak position (Å) | | |
|---|---|---|---|---|---|---|
| System | This work | BKS/BM | exp. | This work | BKS/BM | exp. |
| AS30 | 1.64 (1.65) | (1.53) | 1.68 | 3.17 (3.19) | (3.11) | 3.11 |
| AS50 | 1.68 (1.78) | (1.52) | 1.70 | 3.16 (3.18) | (3.16) | 3.16 |
| AS70 | 1.72 (1.76) | 1.62 (1.52) | 1.72 | 3.16 (3.27) | 2.71 (3.14) | 3.16 |

TABLE III: Position of the first and second peak of the total pair-correlation function for AS30, AS50 and AS70 at $T = 2300$ K. MD results of this work are compared with the BKS potential[35], the BM potential[39] and experimental data (exp.)[50]. Number in parenthesis correspond to simulations at $T = 3500$ K.

data of Wilding *et al.*[50]. Our results are also compared with simulations of Winkler *et al.*[35] based on the BKS potential[43] as well as those of Van Hoang[39] using a Born-Mayer (BM) potential, namely Eq. (1) without the contributions of the dipolar expansion[58]. An overall good agreement is found between the BMH potential and the experiments, and even if the height of the first peak is generally overestimated, its position is well reproduced. Moreover, the second and subsequent oscillations reproduce very well the experimental data, which is consistent with the good agreement found at the level of the first sharp diffraction peak in $S(q)$ in Fig 1(a). For AS70, the BMH potential clearly improve the results obtained with the BKS one. Comparing the BMH potential with the BM one[39] at $T = 3500$ K for the three compositions, it is seen that the height of the first peak is comparable, while the position given by the BM potential is significantly shorter. Increasing the temperature from 2300 K to 3500 K results in a slight increase of the first and second peak positions, as can be seen quantitatively in Table III, due to the thermal expansion. Then, we can conclude that the BMH potential is more suitable for the description of the structural properties.

The Fig. 3(a) and (b) show the partial pair-correlation functions of oxide pairs for all compositions at $T = 2300$ K. For the Si-O pairs in Fig 3(a), the position of the first peak for pure Silica, corresponding to the average Si-O bond length, takes the value of 1.62 Å in very good agreement with *ab initio* simulations[60,61], but slightly overestimates the experimental value of $1.58 - 1.60$ Å[62]. With increasing $x$, the Si-O bond length remains essentially unchanged while its height undergo only a slight decrease, showing the strong nature of the Si-O covalent bonding. As a result $g_{Si-O}(r)$ remains essentially zero between 2

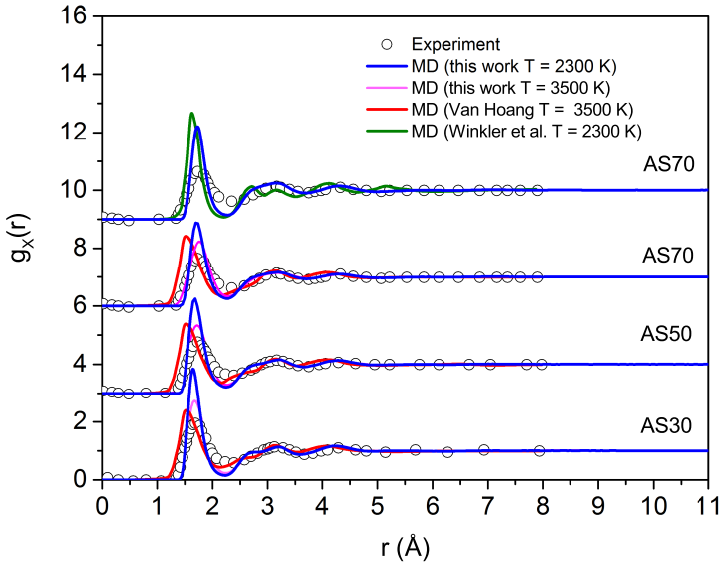


FIG. 2: Total pair-correlation function from X-ray diffraction at $T = 2300$ K for composition AS30, AS50, and AS70. The open circles are the experimental data of Wilding *et al.*[50] between 2200 K and 2300 K, while the full blue lines are the simulation data of the present work. The results of the present work are also compared with the MD simulation data of Winkler et al.[35] (full green line) at $T = 2300$ K for AS70 in the upper curves, and Van Hoang[39] at $T = 3500$ K for AS30, AS50, and AS70.

to 2.5 Å, revealing that Si-O bond breaking is rare. $g_{Al-O}(r)$ in Fig. 3(b) shows a first peak position for pure liquid alumina at 1.74 Å, in good concordance with experiment[63] (1.78 Å) and *ab initio* MD for the amorphous phase[64] (1.80 Å), which is expected to be not very different from the value in the liquid. The evolution with $Al_2O_3$ composition of $g_{Al-O}(r)$ shows features similar to $g_{Si-O}(r)$, however the first peak height is lower and broader with non-zero values between the first and second peak, indicating that the Al-O covalent bond is weaker than Si-O one and is more subject to bond-breaking. Fig. 3(c) displays the evolution of the O-O pairs with composition, which is significant. The first peak position shift to greater values with increase $Al_2O_3$ content. It takes the value of 2.64 Å for $SiO_2$, close to the *ab initio* value[60] of 2.62 Å and increase gradually to 2.75 Å for $Al_2O_3$ in agreement with the value of 2.8 Å expected from *ab initio* calculations[64]. Such an evolution should have an impact on the network topology that will be investigated below. Fig. 3(d) the Al-Si

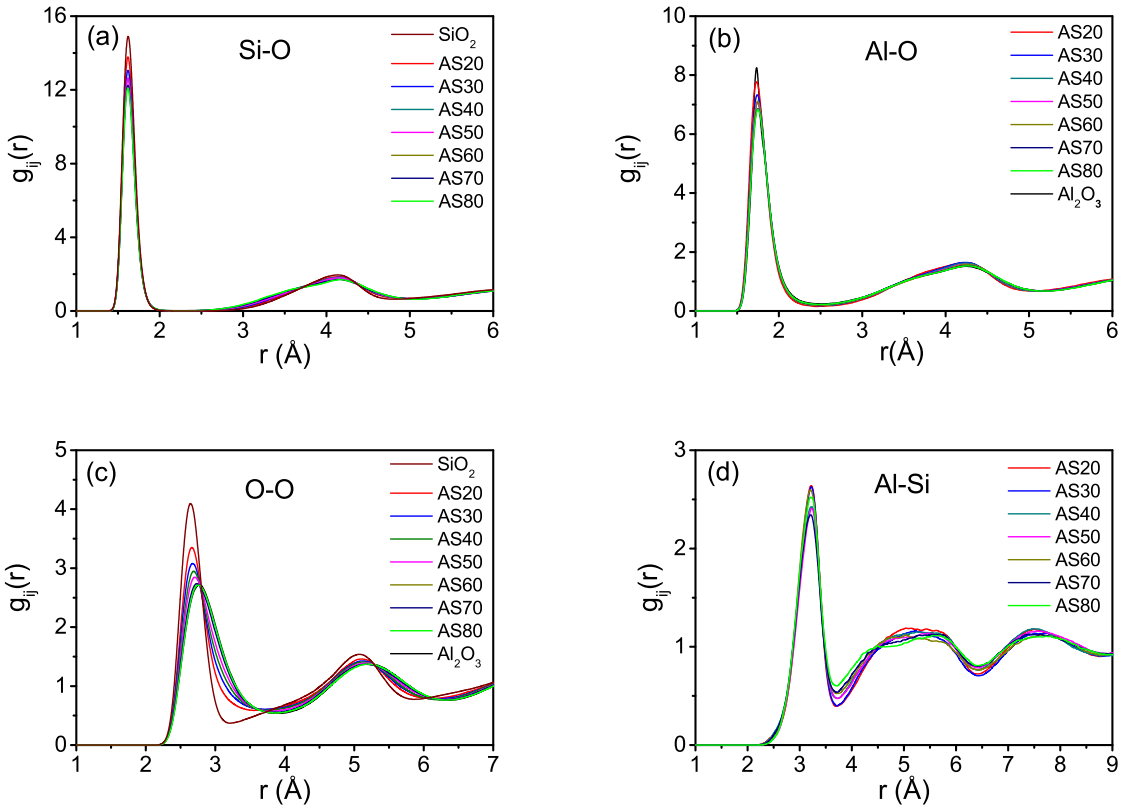


FIG. 3: Partial pair-correlation functions at $T = 2300$ K for all compositions: (a) Si-O, (b) Al-O, (c) O-O, and (d) Al-Si.

pair-correlation function that gives information about triclusters (TBO) geometry with a typical cation-cation distance of 3.22 Å. As can be seen, no specific evolution occurs with $x$.

We come now to the Oxygen environment revealed through the average coordination number, which is shown in Fig. 4 for temperature $T = 2300$ K. It has been determined by counting the number of Al and Si atoms within a sphere of radius 2.5 Å corresponding to the minimum of the Al-O and Si-O pair-correlation functions. An increase with composition from a value of 2 for pure Silica to a value of 3 for pure Alumina is seen, in excellent agreement with experiment. Again, this shows the transferability of the BMH potential to AS systems for all compositions, and comparing our results to those obtained with the BM potential[39] reveal improvements obtained especially for high $Al_2O_3$ contents. The value of 2 for pure Silica is a characteristic feature of corner sharing $SiO_4^+$ tetrahedral network[60]. With increasing $x$, Si atoms are progressively replaced by Al atoms as can be seen on the evolution

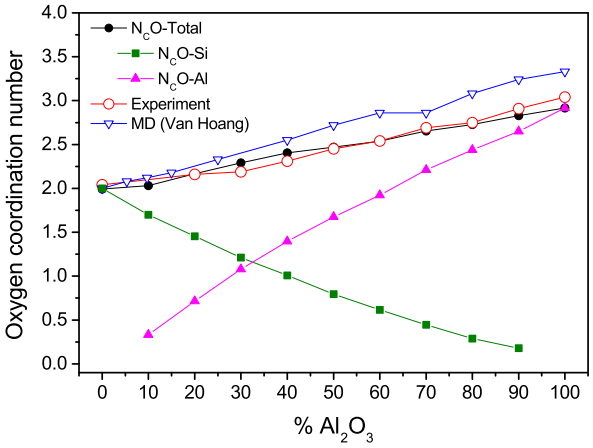


FIG. 4: Coordination numbers around Oxygen atoms at $T = 2300$ K a function of compositions.

of the partial coordination numbers $N_C-$(O-Si) and $N_C-$(O-Al), and accompanied by an increase of the Oxygen coordination above 2. This indicates that the network structure becomes more complex with a significant amount of O atoms surrounded by more than two cations.

A deeper insight into the evolution with composition of the network topology is obtained by considering first the distribution of coordination numbers around Si and Al atoms as shown respectively in Fig. 5(a) and (b). Whatever the composition, nearly 99% of Si atoms are surrounded by 4 O atoms due to the strong Si-O covalent bonding. This feature was also observed in other systems like CAS[16,28,29] and Calcium Silicate[65]. The remaining $\sim 1\%$ of the Si atoms are threefold and fivefold coordinated and form transiently as a mechanism of atomic diffusion[60,66]. Then, we do not observe the emergence of a steady amount of $SiO_5$ with increasing $x$, contrarily to was hypothesized from early combined experimental and simulation results[19].

On the contrary, the number of O atoms around Al is distributed between 3 and 6. Firstly, whatever the concentration, $AlO_4$ remain the most numerous structural units (more than 70%) which is consistent with previous findings for pure Alumina[67] and several AS compositions[35,36]. While the proportion of $AlO_3$ and $AlO_6$ units remain always quite small (below 10%), that of $AlO_5$ ones is more significant (between 10 and 25%). Secondly, looking at their evolution with $x$, the main feature is an increase of the $AlO_5$ units at the expense of the $AlO_3$ and $AlO_4$ ones. The progressive increase of the $AlO_5$ with a significant proportion

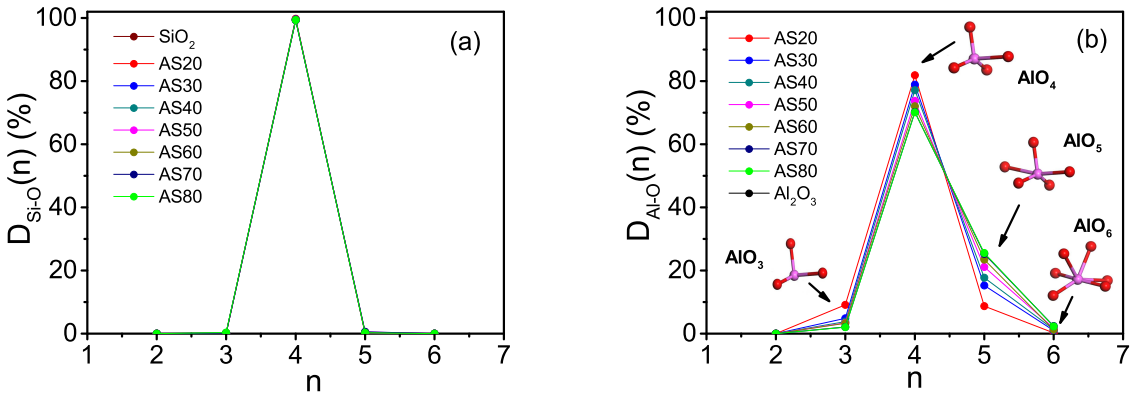


FIG. 5: Distribution of the number $n$ of Oxygen around Si (a), and Al atoms (b) for all compositions at $T = 2300$ K. In panel (b), insets show atomic structures representative of $AlO_5$ and $AlO_6$ (O is in red color and Al in violet).

corresponds to the observations by Al Nuclear Magnetic Resonance Spectroscopy[18] in the melt and also to those in the glass[27] for compositions higher than 5%. In the limiting case of Alumina, the proportions of $AlO_3$, $AlO_4$, and $AlO_5$ found here are quite similar to those found by Gutierrez *et al.*[67]. However, the proportion of $AlO_4$ overestimate those found in a very recent experimental and numerical contribution[68] $(56-63\ \%)$ while in underestimates their proportions of $AlO_5$ $(24-37\ \%)$. From our results, the average Al coordination number increases from 4.001 for AS10 to 4.285 for pure Alumina.

As shown in Fig. 4, the present simulations indicate a coordination around O atoms over 2 whatever the $Al_2O_3$ concentration which implies the formation, in non negligible proportion, of oxygen triclusters (TBO). By definition, TBO consist of three-fold coordinated oxygen atoms with 3 Al (O-3Al), 2 Al and 1 Si (O-2AlSi), 1 Al and 2 Si (O-Al2Si), or 3 Si (O-3Si) atoms without restrictions on the geometrical nature of the local environment around the three cations linked to them. Fig. 6(a) shows the evolution of TBO as function of $x$ at temperature $T = 2300$ K. The abundance of TBO with respect to the total number of O atoms increases monotonically with concentration. They are essentially formed by O-3Al and O-2AlSi entities, while O-3Si and O-Al2Si ones are negligible (this is logically due to the strength of the SiO4 network) and are therefore not drawn. The introduction of $Al_2O_3$ compound induces a progressive replacement of Si by Al atoms in the Silica network and the formation of O-2AlSi TBO up to 30% $Al_2O_3$. This is concomitant to the formation of

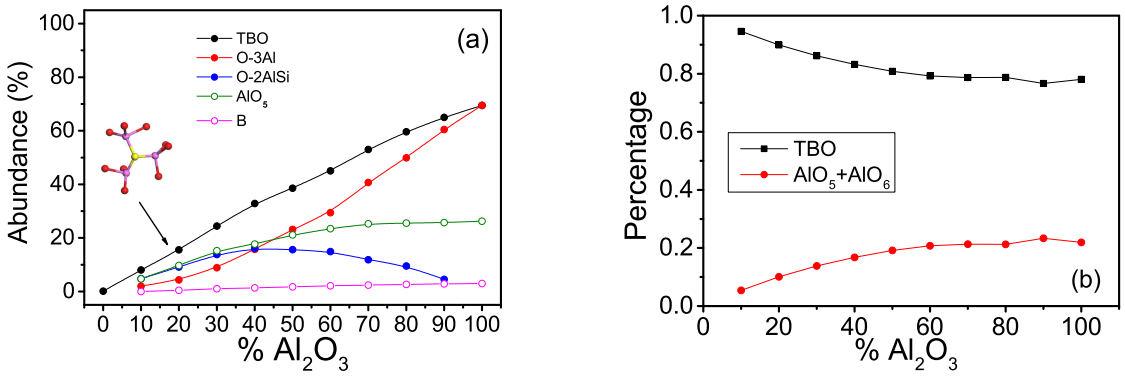


FIG. 6: (a) Evolution of the abundances of triclusters, $AlO_5$ and $AlO_6$ structural units as a function $Al_2O_3$ composition at $T = 2300$ K. The Insert shows a typical representation of O-3Al tricluster (central O atom in yellow color, O in tetrahedral $AlO_4$ units in red color, and Al in violet color).(b) Evolution with composition of the percentage of triclusters and AlO5 + AlO6 with respect to the total amount of them.

increasing proportion of $AlO_5$ and $AlO_6$ units (the latter remain always below 3%) which are also shown in Fig. 6(a). At 30% and above, the number Al atoms becomes sufficient to start forming significantly O-3Al TBO. At 40%, Al atoms become in the majority, as can be seen in Table II, yielding a decrease of the O-2AlSi TBO and therefore a more pronounced rise of the O-3Al TBO.

As mentioned above, the large majority of the structural units around Al atoms are $AlO_4$, which implies a charge balancing by either TBO or by $AlO_5$ and $AlO_6$. From Fig. 6(b), this charge balancing is insured more than 80% by TBO. Moreover, as the $Al_2O_3$ composition decreases to zero, the percentage of TBO rise to 100%. Sen and Youngman[27] hypothesized from their experimental results in the glassy state that charge balancing in fulfilled by the TBO at very low concentration ($< 1$wt%) and by $AlO_5$ and $AlO_6$ at higher concentrations. Our results are in line with this hypothesis at very low concentration, however for higher ones, Fig. 6(b) shows that the formation of TBO remains the main mechanism for charge compensation for all compositions.

Finally, we highlight in Fig. 7 the geometrical nature of the structural units studied above from the bond angle distribution. The latter is calculated using the same cutoff radii as for the coordination numbers. Fig. 7(a) shows the O-Si-O angular distribution with a single

peak centered on 109° which does not change with $x$. As the large majority of Si atoms are four-coordinated atoms, the $SiO_4$ entities adopt a tetrahedral shape. At low values of $x$, Oxygen atoms are twofold coordinated indicating that Si atoms form a strong corner-sharing tetrahedral network. In Fig. 7(b), the O-Al-O distribution is more complex and show a significant evolution with composition. The main peak of the angular distribution evolves from 107° at low $Al_2O_3$ concentration toward 97° for pure alumina, indicating that the tetrahedral structure becomes more and more distorted. Moreover, an additional hump around 165° shows up, which might be associated with the increase of $AlO_5$ units. The Al-O-Al and Al-O-Si distributions shown in Fig. 7(c) and (d) are characteristic of the link between $AlO_x$ units and between $AlO_x$ and $SiO_4$, respectively. The Al-O-Al distribution shows two maxima, the first one located around 91° and the second one around 116°. As shown in the insets, the first corresponds to the formation of edge sharing tetrahedra while the second is characteristics of the formation of triclusters. The Al-O-Si distribution shows also two maxima, one similarly around 91°, while the second one is broader and centered at larger distances, namely 130° corresponding to various geometrical situations including corner-sharing tetrahedra and triclusters. For both distributions, with addition of $Al_2O_3$ content, the amplitude of the peak located around 91° decrease while the one located at larger angles increases.

Then the structural image emerging from this analysis is the progressive formation of $AlO_5$ and $AlO_6$ as well as triclusters as $x$ increases. The strong edge-sharing tetrahedral structure in $SiO_2$ is weakened *i.e* it undergo a so-called depolymerization first by forming edge-sharing tetrahedra, and then at higher concentration triclusters and $AlO_5$ structural units that maintains the charge balancing. This structural entities might then play a role in the dynamic properties and the fragility as was observed in the CAS compounds[12,16,28].

### B. Dynamic properties

Before analyzing the dynamical behavior as well as the fragility as a function of composition, the determination of the glass transition temperature for each composition is needed. This is carried out within the Potential Energy Landscape (PEL) concept[69,70]. As was done in our previous work[16], for each composition, the Inherent Structure Energies (ISE) are first determined as a function of temperature by mean of a conjugate gradient minimization to

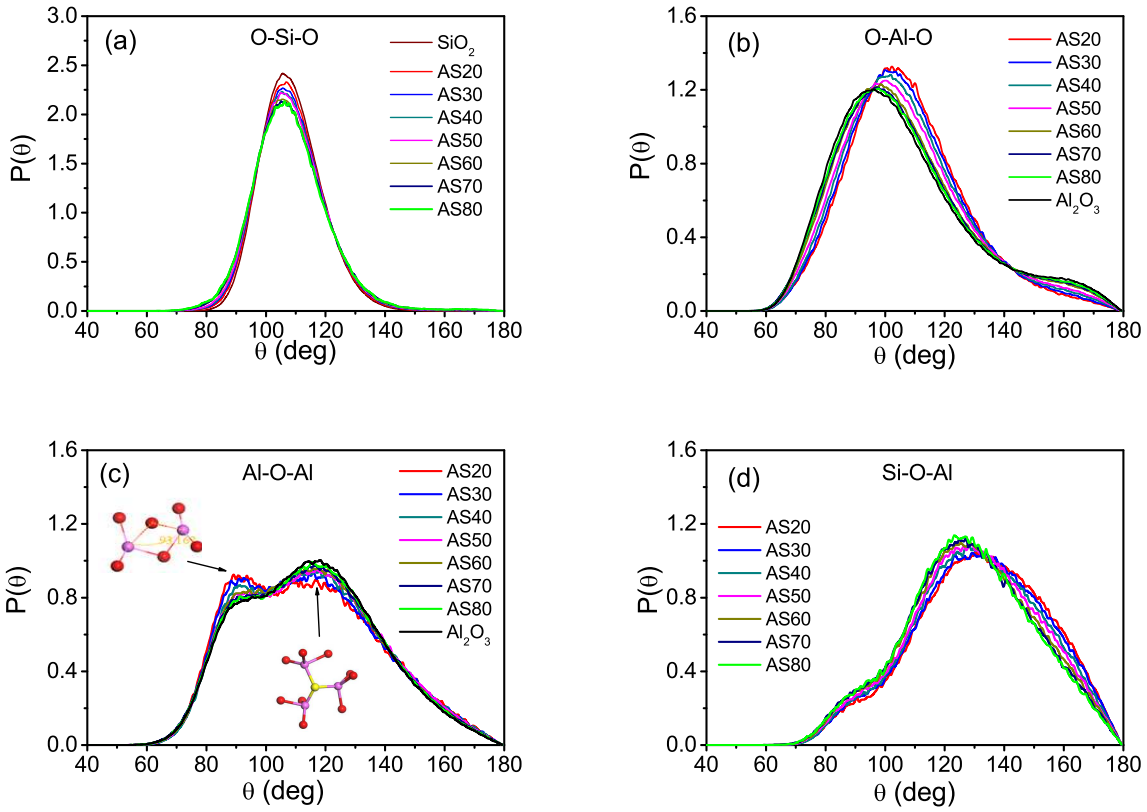


FIG. 7: Bond-angle distribution of (a) O-Si-O, (b) O-Al-O, (c) Al-O-Al, (d) Al-O-Si at temperature $T = 2300$ K for all compositions. Inset in panel (c) shows typical structural units with angle Al-O-Al and Al-O-Si, respectively.

bring the system on the PEL. 50 configurations are minimized to get an averaged ISE for each temperature and composition. The ISE are shown in Fig. 8(a) only for three compositions for the sake of clarity. The curves have been shifted with respect to their value at $T = 300$ K. In the high temperature regime above 4000 K, the ISE shows a rather weak slope, which corresponds to a diffusive regime, and in this case, the kinetic energy is large enough to explore a sufficient proportion of local minima of the PEL. As the temperature decreases, lower energy minima are progressively explored. At temperatures below $T = 4000$ K the ISE starts to decrease more rapidly, and the systems enter the so-called landscape influenced regime where the system is unable to jump over the highest energy barriers. As a result, it gradually gets trapped in deeper energy minima. Finally, the ISE becomes nearly constant at low temperatures, and the system can be considered as having found a single

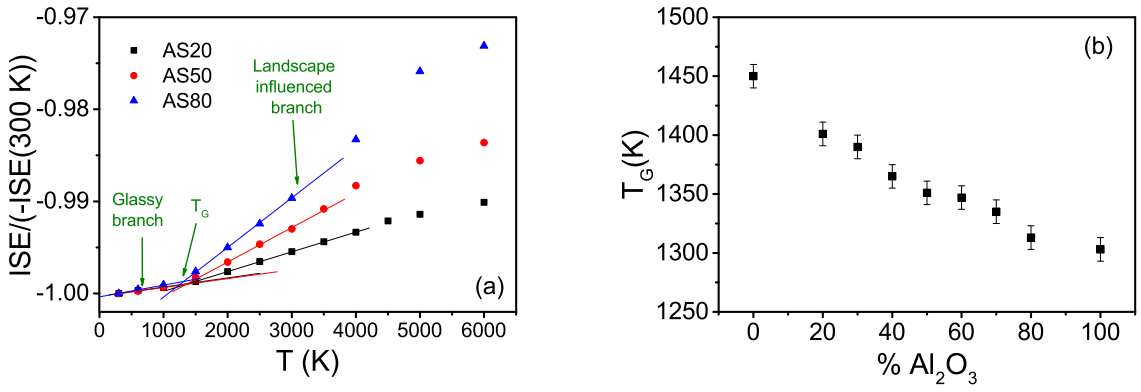


FIG. 8: (a) Inherent structure energy (ISE) as function temperature for composition AS20, AS50 and AS80 scaled with respect to that at 300 K. The crossover between landscape influenced branch and glassy branch defines the glass transition temperature $T_G$. (b) Glass temperature transition as function $Al_2O_3$ composition.

minimum and therefore experience a glassy behavior. The value of $T_G$ is then obtained from the crossover between the landscape influenced branch curve and the glass branch of the ISE. From the uncertainty of the slope of the linear fits, the error bars on the value of $T_G$ are estimated to be of the order of 30 K. The evolution of $T_G$ as a function of composition is shown in Fig. 8(b). As can be seen, the value of $T_G$ decreases with increasing $x$, which is consistent with the progressive depolymerization of the $SiO_2$ tetrahedral network as discussed in the preceding section.

The resulting effect of the weakening of the tetrahedral network on the dynamics can be first seen on the self-diffusion coefficient of the different species, which are drawn in Fig. 9 for two temperatures as a function of composition. As a matter of fact, an increase of the diffusivity occurs as $x$ increases. Interesting enough, the values of $D$ for Oxygen atoms is intermediate between those of Al and Si, which is consistent with the fact that O is more tightly bound to the slower Si atoms. As the $Al_2O_3$ composition increases, the Si atoms becomes progressively in the minority and consequently the diffusion of Oxygen becomes closer to that of Al.

We come now to the temperature evolution of the self-diffusion coefficient of Oxygen, $D_O$, which is then characteristic of the diffusivity in the system. Fig. 10 shows the Arrhenius plot of $D_O$ in the liquid and undercooled region. As can be seen, for all compositions, $D_O$

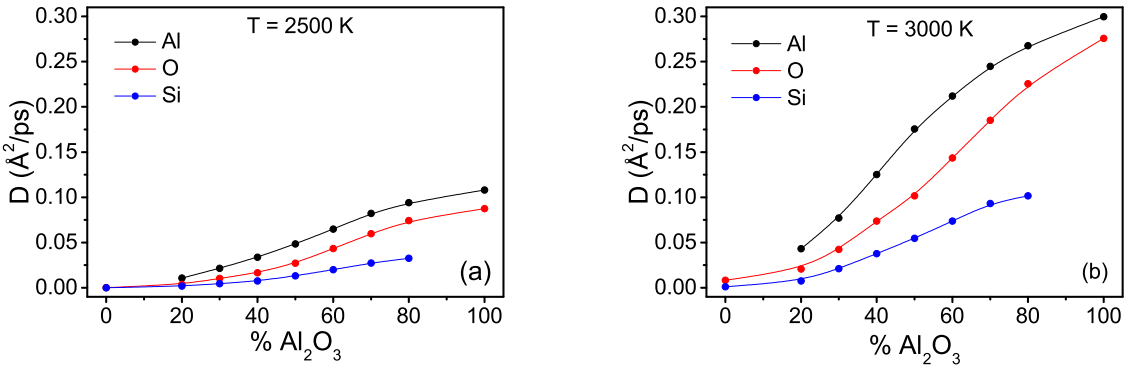


FIG. 9: Self-diffusion coefficients of the three species as function of $Al_2O_3$ composition at (a) 2500 K and (b) 3000 K.

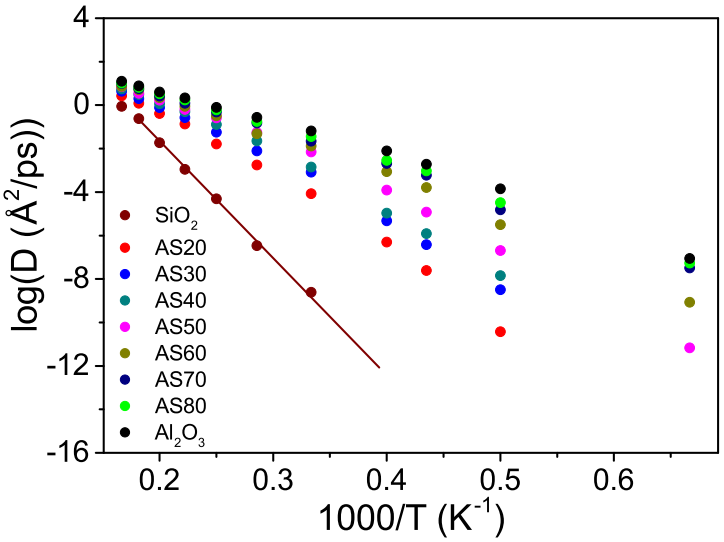


FIG. 10: Arrhenius plot of Oxygen Self-diffusion coefficient in the whole range of compositions.

shows an non-Arrhenius behavior except for pure $SiO_2$ for which $D_O$ crossovers towards an Arrhenius law in the low temperature regime $D = D_\infty exp(-E_a/k_BT)$. This feature has been observed also using the BKS potential[35,36]. The activation energy $E_a$ for pure Silica for Oxygen diffusion is 477 kJ/mol and compares well with the one for the viscosity (see below) with a value of 487 kJ/mol and agrees quite well with the experimental value (514 kJ/mol)[72].

Fig. 11(a) represents the Arrhenius plot of the viscosity calculated from the RNEMD

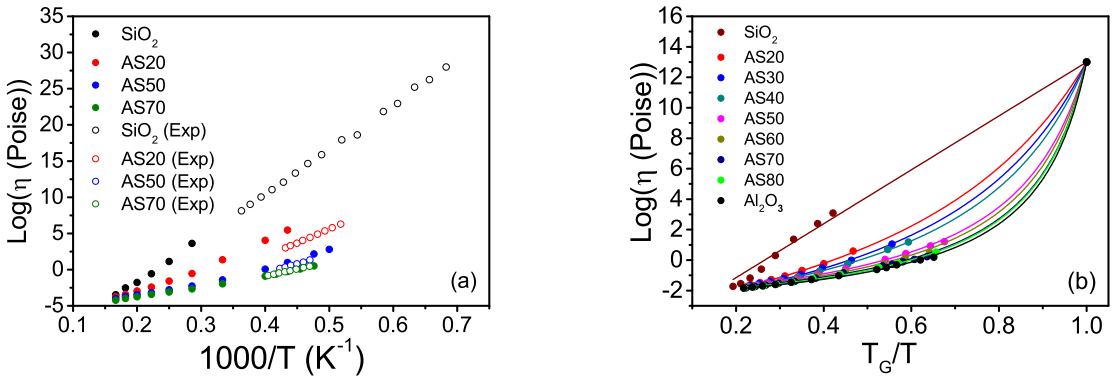


FIG. 11: (a) Evolution of the viscosity as function of inverse temperature, full circles represent our MD simulation results and open circles are the experimental data[72]. (b) Angell plot of the viscosity. The full symbols are the simulation data, and the full lines of the same color are the VFT fits.

method and compared with the experimental data of Urbain *et al.*[72] for AS20, AS50, AS70 and $SiO_2$. The viscosity has been calculated down to the lowest possible temperatures. Below, the slope of the velocities profiles is too small to obtain accurate viscosity values, as already mentioned in Section II. A good agreement is found for AS70 while it is reasonable for AS50 and $SiO_2$. For the latter, the lowest temperature for which is was possible to determine the viscosity is higher than the highest experimental one, however both curves follow an Arrhenius law with a similar activation energy. Finally, for AS20 the simulation values overestimate significantly the measurements. We can conclude that this potential is reliable for the calculation of the viscosity for most concentrations except for some low $Al_2O_3$ content systems around $y = 20\%$.

The temperature evolution of the viscosity for all the investigated compositions are shown in Fig. 11(b) in the form of an Angell plot[73], namely as function of the relative temperature $T_G/T$, where $T_G$ is the glass transition temperature. It is found that the simulations data can be described adequately in the whole range of temperature, including the values of $T_G$ determined above from the ISE curves, by law Vogel-Fulcher-Tammann (VFT)

$$\eta(T) = \eta_0 \exp(\frac{BT_0}{T - T_0}). \tag{4}$$

Parameters $\eta_0$, $B$ and $T_0$ are fitted on the simulation data. $T_0$, the so-called Vogel temperature for which the viscosity diverges, is always lower than $T_G$. We mention that the value

| | $T_0$ (K) | $B$ | $m$ |
|---|---|---|---|
| $SiO_2$ | – | 52 | 18 |
| AS20 | 933 | 18.61 | 48.28 |
| AS30 | 1012 | 13.72 | 58.72 |
| AS40 | 1052 | 10.77 | 68.63 |
| AS50 | 1145 | 6.32 | 100.16 |
| AS60 | 1160 | 5.67 | 110.5 |
| AS70 | 1174 | 4.79 | 125.92 |
| AS80 | 1178 | 4.75 | 173.93 |
| $Al_2O_3$ | 1183 | 4.32 | 200.12 |

TABLE IV: Parameters of VFT fit $B$ and $T_0$ and fragility $m$.

of the viscosity at the calculated $T_G$ is taken as the conventional value $\eta = 10^{12}$ Pa.s. From the VFT curves, we have inferred the fragility index which is the slope of the VFT curve at $T_G$, which can be written in terms of the VFT parameters as follows

$$m = \frac{BT_0T_G}{2.3(T_G - T_0)^2}. \tag{5}$$

The values of $m$ span from 15 for strong liquids, where the VFT law reduced to the Arrhenius law, to 200 for fragile ones with a non-Arrhenius behavior. As can be seen on Fig. 11(b), only Silica displays a strong character associated to an Arrhenius law. Table IV gathers the values of $B$ and $T_0$ obtained for the fit of the simulation data together with the fragility index $m$. The latter shows a monotonic increase, indicating that AS liquids become gradually more fragile with increasing $Al_2O_3$ composition. This result might be correlated with the progressive increase of $AlO_5$, $AlO_6$ and TBO strutural units, which induce a depolymerization of the strong corner-sharing tetrahedral structure in $SiO_2$.

## IV. CONCLUSION

In summary, we have studied the structural and dynamics properties of Aluminosilicate $(Al_2O_3)_x$-$(SiO_2)_{1-x}$ melts as a function of $Al_2O_3$ concentration $x$ varying from 0 to 1. For this purpose we have performed classical molecular dynamics simulation using a Born-Mayer-Huggins potential proposed recently by Bouhadja *et al.*[16,28,29] and initially developed for

Calcium Aluminosilicate (CAS) glass-formers.

Firstly, in describing properties such as the total X-ray structure factor, pair-correlations functions, coordination numbers, and viscosity we have found that the BMH potential gives a reasonable description with respect to the available experimental data in the whole concentration range and mainly even more reliable results than the Born-Mayer and van Beest *et al.* potentials currently used. We can conclude that the BMH shows a reasonable transferability from the CAS ternary system to the binary AS one, and also as a function $Al_2O_3$ concentration. For pure substances, Silica and Alumina the transferability is less obvious for the properties considered here and will require further attention.

Given the reliability of this potential, we have shown that the structural image emerging from our study is the progressive formation of $AlO_5$ and $AlO_6$ as well as triclusters with increasing $Al_2O_3$ concentration leading to the progressive weakening or depolymerization the strong corner-sharing tetrahedral structure in $SiO_2$. Our findings also indicate that the charge balancing during this process is mostly insured by Oxygen triclusters.

Consequences of this feature are the decrease of the glass transition temperature, increase of the diffusion coefficients, decrease of the viscosity and an increase of Angell's fragility with concentration. Our finding then indicate that $AlO_5$, $AlO_6$ as well as triclusters structural units might play an important role in the behavior of the dynamics as a function of composition and temperature for AS glass-formers. Systematic study of micro-segregation of Al rich regions and its relationship with the MRO and dynamic heterogeneities using larger scale Molecular dynamics simulations remains to be done and will be considered in future work.

## V. ACKNOWLEDGEMENT

We acknowledge the CINES and IDRIS under Project N INP2227/72914, as well as CIMENT/GRICAD for computational resources. This work was performed within the framework of the Centre of Excellence of Multifunctional Architectured Materials "CEMAM"

ANR-10-LABX-44-01 funded by the "Investments for the Future" Program.

---

[1] J. F. Stebbins, in *Structure, Dynamics and Properties of Silicate Melts*, edited by J. F. Stebbins, P. F. McMillan, and D. B. Dingwell (Mineralogical Society of America, Washington, DC, 1995), **32**.

[2] H. Bach and D. Krause, *Analysis of the Composition and Structure of Glass and Glass Ceramics* (Springer, Berlin, 1999).

[3] B. O. Mysen, *Structure and Properties of Silicate Melts (Elsevier, Amsterdam*,1988);

[4] S. H. Risbud, R. J. Kirkpatrick, A. P. Taglialavore, and B. Montez, J. Am. Ceram. Soc. **70**, C10 (1987).

[5] I. Farnan and J. F. Stebbins, Science **265**, 1206 (1994).

[6] J. F. Stebbins, S. Kroeker, S. K. Lee, and T. J. Kiczenski, J. Non-Cryst. Solids **275**, 1 (2000).

[7] M. J. Toplis and D. B. Dingwell, Geochim. Cosmochim. Acta **68**, 5169 (2004).

[8] S. K. Lee, Geochimica et Cosmochimica Acta, **69**, 3695, (2005).

[9] 23J. F. Stebbins and Z. Xu, Nature (London) **390**, 60 (1997).

[10] J. F. Stebbins, E. V. Dubinsky, K. Kanehashi, and K. E. Kelsey, Geochim. Cosmochim. Acta **72**, 910 (2008).

[11] D. R. Neuville, L. Cormier, A. M. Flank, D. de Ligny, J. Roux, and P. Lagarde, Am. Mineral. **93**, 228 (2008).

[12] N. Jakse, M. Bouhadja, J. Kozaily, J. W. E. Drewitt, L. Hennet, D. R. Neuville, H. E. Fischer,V. Cristiglio, and A. Pasturel, Appl. Phys. Lett. **101**, 201903 (2012).

[13] B. Guillot, N. Sator, Geochimica et Cosmochimica Acta, **71**, 1249-1265 (2007).

[14] K. Li, M. Bouhadja, R. Khanna, J. Zhang, Z. Liu, Y. Zhang, T. Yang, V. Sahajwalla,Y. Yang, M. Barati, Fuel **186**, 561–570 (2016).

[15] K. Li, R. Khanna, M. Bouhadja, J. Zhang, Z. Liu, B. Su, T. Yang, V. Sahajwalla, C. V. Singh, M. Barati, Chem. Eng. J. **313**, 1184-1193 (2017).

[16] M. Bouhadja, N. Jakse, and A. Pasturel, J. Chem. Phys. **140**, 234507 (2014).

[17] R. K. Sato, P. F. McMillan, P. Dennison, and R. Dupree, J. Phys. Chem. **95**, 4483 (1991).

[18] B. T. Poe, P. F. McMillan, B. Coté, D. Massiot, and J.-P. Coutures, J. Phys. Chem. **96**, 8220 (1992).

[19] B. T. Poe, P. F. McMillan, C. A. Angell, and R. K. Sato, Chem. Geol. **96**, 333 (1992).

[20] R. H. Meinhold, R. C. T. Slade, and T. W. Dawies, Appl. Magn. Reson. **4**, 141 (1993).

[21] M. Schmücker and H. Schneider, Ber. Bunsenges. Phys. Chem. **100**, 1550 (1996).

[22] M. Schmücker, K. J. D. MacKenzie, H. Schneider, and R. Meinhold, J. Non-Cryst. Solids **217**, 99 (1997).

[23] M. Schmücker, H. Schneider, K. J. D. MacKenzie, and M. Okuno, J. Eur. Ceram. Soc. **19**, 99 (1999).

[24] H. Morikawa, S.-I. Miwa, M. Miyake, F. Marum, and T. Sata, J. Am. Ceram. Soc. **65**, 78 (1982).

[25] P. F. McMillan and B. Piriou, J. Non-Cryst. Solids **53**, 279 (1982);

[26] M. Okuno, N. Zotov, M. Schmücker, and H. Schneider, J. Non-Cryst. Solids **351**, 1032 (2005).

[27] S. Sen and R. E. Youngman, J. Phys. Chem. B, **108**, 7557-7564 (2004).

[28] M. Bouhadja, N. Jakse, and A. Pasturel, J. Chem. Phys. **138**, 224510 (2013).

[29] M. Bouhadja, N. Jakse, and A. Pasturel, Mol. Sim., **40**, 251-259 (2014).

[30] H. Hosono and Y. Abe, J. Am. Ceram. Soc. **70**, C-38 (1987).

[31] D. A. Dutt, P. L. Higby, and D. L. Griscom, J. Non-Cryst. Solids **130**, 41 (1991).

[32] D. A. Dutt, P. L. Higby, and D. L. Griscom, Phys. Chem. Glasses **33**, 51 (1992).

[33] M. P. Allen, D. J. Tildesley. *Computer simulation of liquids*, Oxford Science Publication (1989).

[34] B. Smit, D. Frenkel. *Understanding molecular simulations*, 2nd ed., Academic Press, San Diego (2002).

[35] A. Winkler, J. Horbach, W. Kob, and K. Binder, J. Chem. Phys. **120**, 384 (2004).

[36] P. Pfleiderer, J. Horbach, W. Kob, and K. Binder, Chem. Geol. **229**, 186 (2006).

[37] K. Binder, J. Horbach, H. Knoth, and P. Pfleiderer, J. Phys.: Condens. Matter **19**, 205102 (2007).

[38] V. V. Hoang, N.N. Linh, and N.H. Hung, Eur. Phys. J. Appl. Phys. **37**, 111 (2007).

[39] V. V. Hoang, Phys. Rev. B **75**, 174202 (2007).

[40] N. N. Linh and V.V. Hoang, Phys. Scr. **76**, 165 (2007). .

[41] V. V. Hoang, Phys. Lett. A **368**, 499 (2007).

[42] G. J. Kramer, A. J. M. de Man, and R. A. van Santen, J. Am. Chem. Soc. **113**, 6435 (1991).

[43] van Beest, B.W.H., Kramer, G.J., van Santen, R.A., Phys. Rev. Lett. 64, 1955 (1990).

[44] M. Huggins, J. E. Mayer, J.Chem. Phys., **1**, 643 (1933).

[45] M. Matsui, Miner. Mag. 58A, 571 (1994).

[46] L. T. Mai, Y. V. Nguyen, H. V. Nguyen, and H. K. Pham, Phys. Chem. Liq. **55**, 62 (2017)

[47] T. H. T. Nguyen, Y. V. Nguyen, H. K. Pham and H. V. Nguyen, J. Mod. Phys. B, **31**, 1750127 (2017).

[48] Z. Liu, Y. Hu, X. Li, W. Song, S. Goyal, M. Micoulaut, and M. Bauchy, Phys. Rev. B **98**, 104205 (2018).

[49] H. Jabraoui, M. Malki, A. Hasnaoui, M. Badawi, S. Ouaskit, S. Lebègue, Y. Vaills, Phys. Chem. Chem. Phys. **19**, 19083 (2017).

[50] M. C. Wilding, C. J. Benmore, J. K. R. Weber, J. Phys. Chem. B **114**, 5742-5746 (2010).

[51] X. Dai, J. He, J. Bai, Q. Huang, X. Wen, L. Xie, K. Luo, J. Zhang, W. Li, and S. Du, Energy Fuels **30**, 2407 (2016).

[52] T. K. Bechgaard, J. C. Mauro, M. Bauchy, Y. Yue, L. A. Lamberson, L. R.Jensen, M. M. Smedskjaer, J. Non-Cryst. Solids **461**, 24 (2017).

[53] M. Bauchy, J. Chem. Phys. **141**, 024507 (2014).

[54] S. J. Plimpton, J. Comp. Phys. **117**, 1 (1995); http://www.lammps.sandia.gov.

[55] ISAACS-interactive structure analysis of amorphous and crystalline systems http://isaacs.sourceforge.net/over.html; S. Le Roux, I. Petkov, J. Appl. Cryst. **43**, 181 (2010).

[56] F. Muller-Plathe, Phys. Rev. E. **59**, 4894 (1999).

[57] P. Bordat, F. Muller-Plathe, J. Chem. Phys., **116**, 3362 (2002).

[58] D. K. Belashenko, Russian. Chem. Rev., **66**, 733 (1997).

[59] L. B. Skinner, A. C. Barnes, P. S. Salmon, L. Hennet, H. E. Fischer, C. J. Benmore, S. Kohara, J. K. R. Weber, A. Bytchkov, M. C. Wilding, J. B. Parise, and T. O. Farmer, Phys. Rev. B **87**, 024201 (2013).

[60] J. Sarnthein, A. Pasquarello, and R. Car, Phys. Rev. Lett. **74**, 4682 (1995).

[61] A. Carré, J. Horbach, S. Ispas and W. Kob Europhys. Lett. **82**, 17001 (2008).

[62] C. J. Benmore, E. Soignard, S. A. Amin, M. Guthrie, S. D. Shastri, P. L. Lee, J. L. Yarger, Phys. Rev. B **81**, 054105 (2010).

[63] C. Landron, L. Hennet, T. E. Jenkins, G. N. Greaves, J. P. Coutures, A. K. Soper, Phys. Rev. Lett. **86**, 4839 (2001).

[64] S. Davis and G. Gutierrez, J. Phys.: Condens. Matter **23**, 495401 (2011).

[65] R. N. Mead and G. Mountjoy, J. Phys. Chem. B **110**,14273 (2006).

[66] K. Hung, N. T. T. Ha, M. T. Lan, and N. V. Hong, J. Chem. Phys. **138**, 244505 (2013).

[67] G. Gutierrez, A. B. Belonoshko, R. Ahuja, B. Johansson, Phys. Rev. E **61**, 2723 (2000).

[68] C. Shi, O. L. G. Alderman, D. Berman, J. Du, J. Neuefeind, A. Tamalonis, J. K. R. Weber, J. You and C. J. Benmore, Front. Mater. **6**, 38 (2019).

[69] F. H. Stillinger, Science. **267**, 1935 (1995).

[70] S. Sastry, P.G. Debenedetti, F. H. Stillinger, Nature **393**, 554 (1998).

[71] F. H. Stillinger and T. A. Weber, Phys. Rev. A **25**, 978 (1982).

[72] G. Urbain, Y. Bottinga, P. Richet, Geochimica Cosmochimica Acta, **46**, 1061 (1982).

[73] C. A. Angell, Science 267, 1924 (1995).